Size Dependent Fragmentation Chemistry of Short Doubly Protonated Tryptic Peptides

Shanshan Guan[†,‖] and Benjamin J. Bythell[†,‖*]

[†]Department of Chemistry and Biochemistry, Ohio University, 307 Chemistry Building, Athens, OH 45701

[‖]Department of Chemistry and Biochemistry, University of Missouri-St. Louis, 1 University Blvd, St. Louis, MO 63121

ABSTRACT: Tandem mass spectrometry of electrospray ionized multiply charged peptide ions is commonly used to identify the sequence of peptide(s) and infer the identity of source protein(s). Doubly protonated peptide ions are consistently the most efficiently sequenced ions following collision-induced dissociation of peptides generated by tryptic digestion. While the broad characteristics of longer ($N \geq 8$ residue) doubly protonated peptides have been investigated, there is comparatively little data on shorter systems where charge repulsion should exhibit the greatest influence on the dissociation chemistry. To address this gap and further understand the chemistry underlying collisional-dissociation of doubly charged tryptic peptides, two series of analytes ($[G_xR+2H]^{2+}$ and $[A_xR+2H]^{2+}$, x=2-5) were investigated experimentally and with theory. We find distinct differences in the preference of bond cleavage sites for these peptides as a function of size and to a lesser extent composition. Density functional calculations at two levels of theory predict that the threshold relative energies required for bond cleavages at the same site for peptides of different size are quite similar (for example, b_2-y_{N-2}). In isolation, this finding is inconsistent with experiment. However, the predicted extent of entropy change of these reactions is size dependent. Subsequent RRKM rate constant calculations provide a far clearer picture of the kinetics of the competing bond cleavage reactions enabling rationalization of experimental findings. M06-2X data were substantially more consistent with experiment than were B3LYP data.

Introduction

Tandem mass spectrometry (MS/MS) of is by far the most widely used method in large scale peptide/protein identification [1–3]. In mass spectrometry-based peptide sequencing, specific mass-to-charge (m/z) ranges corresponding to individual protonated peptide ion types are isolated in the gas-phase, activated, then fragmented. The resulting product ions and remaining precursor ions are then detected. The most used fragmentation method is collision-induced dissociation (CID). Low energy collisions (typically <50 eV per collision in the laboratory frame) with an inert gas, such as helium, nitrogen, or argon transfer energy thereby enabling proton mobilization [4–8] and bond cleavages characteristic of the isolated analyte ion. For most peptides, the least energetically demanding bond cleavages correspond to amide bonds. These peptide fragmentation reactions [1–3, 9, 10] produce several different kinds of peptide sequence informative ion [11] resulting in b_n, a_n and y_m ion series (for an N=n+m residue peptide). As peptides are heteropolymers, the difference in m/z of consecutive ions from each of these series correspond to individual amino acid masses [3]. In optimal cases one can immediately read off the entire peptide sequence from these experiments.

In proteomics studies, analyses typically begin from proteins. Proteins are typically enzymatically digested to form peptides then separated by liquid chromatography prior to MS/MS analysis. Chemical digestion generates shorter peptides which are easier to sequence individually, but at the cost of a substantial increase in the number of analytes to sequence. Consequently, tandem mass spectrometry is routinely coupled to a (preceding) separation techno logy thereby enabling individual analyses of more of the generated peptide mixture. Trypsin remains the most common choice of digestion enzyme. Trypsin cleaves at the carboxyl terminal of lysine (K), or arginine (R), except when either is followed by a proline (P). Peptides generated

by trypsin digestion often form doubly charged peptide ions during the electrospray ionization (ESI) process. Peptide sequence assignments are least error-prone when arrived at from MS/MS spectra of doubly charged tryptic peptide ions [3]. Amide bond cleavage produce b_n ions if the charge(s) is (are) retained by the N-terminal fragment and/or y_m ions [12] when the C-terminal fragment keeps the charge(s). Real MS/MS spectra of peptides do not always produce uninterrupted sequences of b_n or y_m ions.[1–3, 9, 10, 13] Additionally, the presence of satellite ions resulting from loss(es) of small neutrals (NH_3, H_2O) and/or more complex intramolecular rearrangements can complicate sequence assignment further. [1–3, 9, 10, 13]

Peptide sequencing algorithms, such as Mascot [14], X!Tandem [15], and SEQUEST [16], assign peptide sequence by matching the experimental fragment ion m/z values to theoretical MS/MS spectra. These spectra are produced from candidate peptides in protein databases or translated nucleotide databases. One limitation of these algorithms is that they assume the fragment ions of a given type in a theoretical spectrum exhibit the same abundance regardless of the properties of the peptides. [9, 13] For longer (N >12), well behaved peptides, this omission has little cost as the likelihood of a long sequence of random noise matching the m/z values sufficiently well is very low. For shorter peptides, this choice is more problematic. E.g., for some neuropeptides and metabolite peptides.[17] Including the abundance information can potentially improve the confidence of peptide identification because the abundance of each fragment ion depends on the size, charge state, and amino acid composition of the peptide.[9, 18] A major stumbling block to such an approach is an inadequate ability to predict these abundances in the first place. One route to solving such a problem is an improved understanding of gas-phase peptide fragmentation chemistry. Alternate approaches such as spectral libraries [19–22], machine learning [18, 23–27], or statistical modelling [28, 29] are also potential means. For example, (1)

Wysocki and coworker's SeQuence IDentfication (SQID) algorithm, made rough predictions of fragment ion intensity based on statistical analysis of the probability of fragmentation for each amino acid pair in large MS spectra databases [30, 31] and (2) Zhang [28, 29] proposed a kinetic model which estimates the rate constant for each competing fragmentation pathway as well as the abundance of the corresponding fragment ions to predict theoretical MS/MS spectra. Zhang and Bordas-Nagy, then Frank found that their intensity simulation methods were computationally intensive and became less accurate as the peptides got larger and more highly charged [32, 33].

Statistical analyses of protonated peptide spectra by multiple groups indicate that many factors affect the fragmentation of peptides including the mass and the charge states of the peptide ion, number of proline residues, proton mobility, number and position of basic residues as well as the type of mass spectrometer used [34–45]. Savitski et al. used Principal Component Analysis to investigate a large validated dataset of doubly protonated tryptic peptide MS/MS spectra.[37] These authors discovered that the spectra could be separated into two distinct spectral classes. Class I spectra are dominated by the secondary amide bond cleavage producing the y_{N-2} peak as the peak with the greatest abundance. In contrast, Class II spectra cover all other spectra and so exhibit a broad distribution of ion abundances with y_{N-4} and y_{N-5} fragments as the most abundant.[37] While Class I peptides were found to be shorter than class II peptides [37, 46, 47], the overriding physical reason(s) for this stark difference have yet to be conclusively identified. More recently, Shen et al.[48] found linear correlations between the N-terminal residue proton affinities and the intensities of y_m ions in tandem mass spectrometry in their data. The work also illustrated potentially useful correlations between the degree of precursor ion degradation and analyte size.

Computational chemistry using density function theory (DFT) to rationalize and predict peptide fragmentation was pioneered by several groups [49–56]; much of this early work concerned small singly protonated systems. Later analyses of larger and more highly charged systems followed. [34, 57–68] Combined guided ion beam MS experimental studies together with theory [69, 70] have supplemented these data for singly protonated aliphatic di and tripeptide systems. Single-system, doubly protonated peptide calculations provided evidence that amide bond cleavage barriers vary with position with a balance of charge-solvation and charge-charge repulsion being set [61, 62, 66]. Paizs and co-authors provided evidence from calculations, infrared multiple photon dissociation (IRMPD) spectroscopy, and hydrogen/deuterium exchange experiments which indicated that the b_2 fragments generated from a series of Class I tryptic doubly protonated peptides of varying composition generated oxazolone b_2 ion structures [62, 63, 71–73]. Other authors provided evidence that b_2 ion structure could vary with peptide composition [74–76]. Haeffner and Irikura developed a threshold peak abundance prediction model based on the relative energies of the various amide nitrogen protonation sites of $[A_8R+2H]^{2+}$ [77]. For their doubly protonated nonapeptide system these authors argued that separation of product ions in the dimer generated following amide bond cleavage could be rate-limiting [77]; an analytical addition to each barrier of 55±6 kJ/mol enabled an improved fit to the experimental data. These authors note that this model is less likely to be accurate for systems with a higher degree of activation as entropic effects should then predominate. i.e., $\Delta G(T_{effective})$ would be more effective at predicting the spectral abundances at higher degree of activation.

One of the weaknesses of early DFT-based approaches is the prevalence of single-system comparisons rather than series. [61, 62, 66, 68, 78] Thus, analyses of series of both experimental spectra and DFT-modeled pathways together, should offer a more complete and thus general

picture. The advent of superior computing power has enabled a reduction in the relatively high computational (time) cost of these approaches. In the present study, we investigate series of relatively short, model doubly protonated peptides, $[G_xR+2H]^{2+}$ and $[A_xR+2H]^{2+}$ (x=2-5, glycine (G); alanine (A)). We utilize tandem mass spectrometry (MS/MS) experiments at systematically varied collision energies to probe the dissociation characteristics as a function of degree of activation. We model the key dissociation chemistries with density functional theory (DFT) calculations at 2 levels of theory and compare these findings to experiment. Lastly, we utilize Rice–Ramsperger–Kassel–Markus (RRKM) statistical rate calculations to provide estimates of the effect of energy and timescale on these reactions as a function of system size, composition, and chemical (DFT) model. We compare these findings to the preceding literature and identify pertinent considerations for analyzing comparatively charge-dense doubly protonated peptide ion structures.

Experimental

The series of G_xR and A_xR (x=2-5) peptides were synthesized by GenScript, Inc (Piscataway, NJ) and used as received. The experimental data were collected using a Bruker MaXis Plus electrospray/quadrupole time-of-flight mass spectrometer (Bruker, Billerica, MA). The peptides were diluted to ~10^{-5} M with acetonitrile/water/formic acid (50/50/0.1%) and then injected into the mass spectrometer at a flow rate of 3 μl min^{-1}. Nitrogen was used as nebulizing, drying, and collision gas. The product mass spectra for each doubly charged peptide were obtained by mass-selecting the appropriate ion with the quadrupole (isolation window 2u) followed by CID in the collision cell, prior to dispersion and detection in the time-of-flight mass analyzer. Data were

collected as a function of collision energy. Breakdown graphs were plotted to illustrate the relative abundance of precursor and fragment ions as a function of collision energy for all species studied.

Theoretical Methods

Initial candidate structures of doubly protonated peptide ions were systematically generated [63, 64, 79] via molecular dynamics using InsightII (Biosym Technologies, San Diego, CA) in conjunction with the AMBER force field [80], and/or the tool Fafoom [81, 82] which is a genetic algorithm which systematically alters bond angles to produce new candidates structures which are then initially optimized using the MMFF94 Force Field.[83–87] Geometry optimizations of the resulting candidate conformations were performed with the Gaussian 09 [88] software package at the HF/3-21G, M06-2X/6-31G(d) or B3LYP/6-31G(d), and B3LYP/6-31+G(d,p) [89, 90], and M06-2X/6-31+G(d,p) [91, 92] levels of theory. Calculations of minima, transition structures (TSs), and product ions (and neutrals) of each reaction pathway were performed. Multiple TS calculations were systematically performed for each reaction pathway type in each system to identify the lowest energy pathways. The reaction pathway through the lowest energy TS of each type was calculated with intrinsic reaction coordinate (IRC) calculations (up to 18 steps in each direction). The resulting structures were then optimized further with small incremental steps.

To gain further insight into kinetic aspects of the competing dissociation processes RRKM calculations were performed using the energetics, vibrational frequencies, and rotational constants derived from the TSs and corresponding global minimum structures to approximate the time scale of the fragmentation reactions [93, 94]. The Beyer-Swinehart algorithm [95] was used to calculate the sum and density of states.

A brief word on DFT models

DFT models seek to describe the exchange-correlation energy accurately. The exchange-correlation energy describes all the components of the system that we cannot presently calculate exactly, the non-classical effects of self-interaction correction, exchange, and correlation. This comprises both contributions to the potential energy of the system and a portion of the kinetic energy. The almost ubiquitous B3LYP model is a hybrid functional that incorporates 20% exact (Hartree-Fock) exchange along with pure density functionals for exchange. A 3-parameter fit against reference data using the Becke (B) exchange [96], and the Lee, Yang and Parr (LYP) correlation functionals [90] produced the remaining parameters. M06-2X also has semi-empirical character and includes multiple parameters generated from fits. However, the functional incorporates far more exact exchange (54%) and utilizes one of Grimme's long-range dispersion corrections.[91, 97] Overall, this parameter set and improved description of long-range interactions has resulted in improved description of dissociation chemistry relative to B3LYP. A good example is in the description of S_N2 reactions where B3LYP has been shown to systematically underestimate barrier heights.[98–102] Even though B3LYP has several known problems, it is still widely used, often successful, and was the model most frequently previously used for doubly protonated peptides. Hence its inclusion here.

Results

1. *Tandem mass spectra of doubly protonated peptides*

Tandem mass spectra series were collected for both analytes series. **Figure 1** illustrates an example spectrum and breakdown graph for the $[A_4R+2H]^{2+}$ analytes (Figure S1 and S2 show $[A_xR+2H]^{2+}$

and $[G_xR+2H]^{2+}$ series at 50% dissociation). MS/MS spectra of both analyte types were dominated by singly charged y_m ion series produced from amide bond cleavages [9]. The nature of the amide bond cleavage process (b_n-y_m vs. a_n-y_m, **Scheme 1**) determines the source(s) of these ions and their corresponding N-terminal peak (b_n and/or a_n) abundances. We detect distinct differences in the preference of bond cleavage sites for these peptides as a function of peptide length and to a lesser extent composition. For example, the shortest, most charge dense analytes far more readily produce abundant y_{N-1} peaks corresponding to the typically more energetically demanding a_1-y_{N-1} amide bond cleavage pathway [9, 52, 103]. Whereas the longer, less charge dense doubly protonated peptides utilize the b_n-y_m pathway primarily, so predominantly produce b_n and y_m ion series. We note that detection of a_1 ions is discriminated against by our (and other) instrument(s) due to their low mass-to-charge; m/z 30, $H_2C{=}NH_2^+$, and 44, $H_3CHC{=}NH_2^+$, (a_1 (immonium) ions of glycine and alanine, respectively).

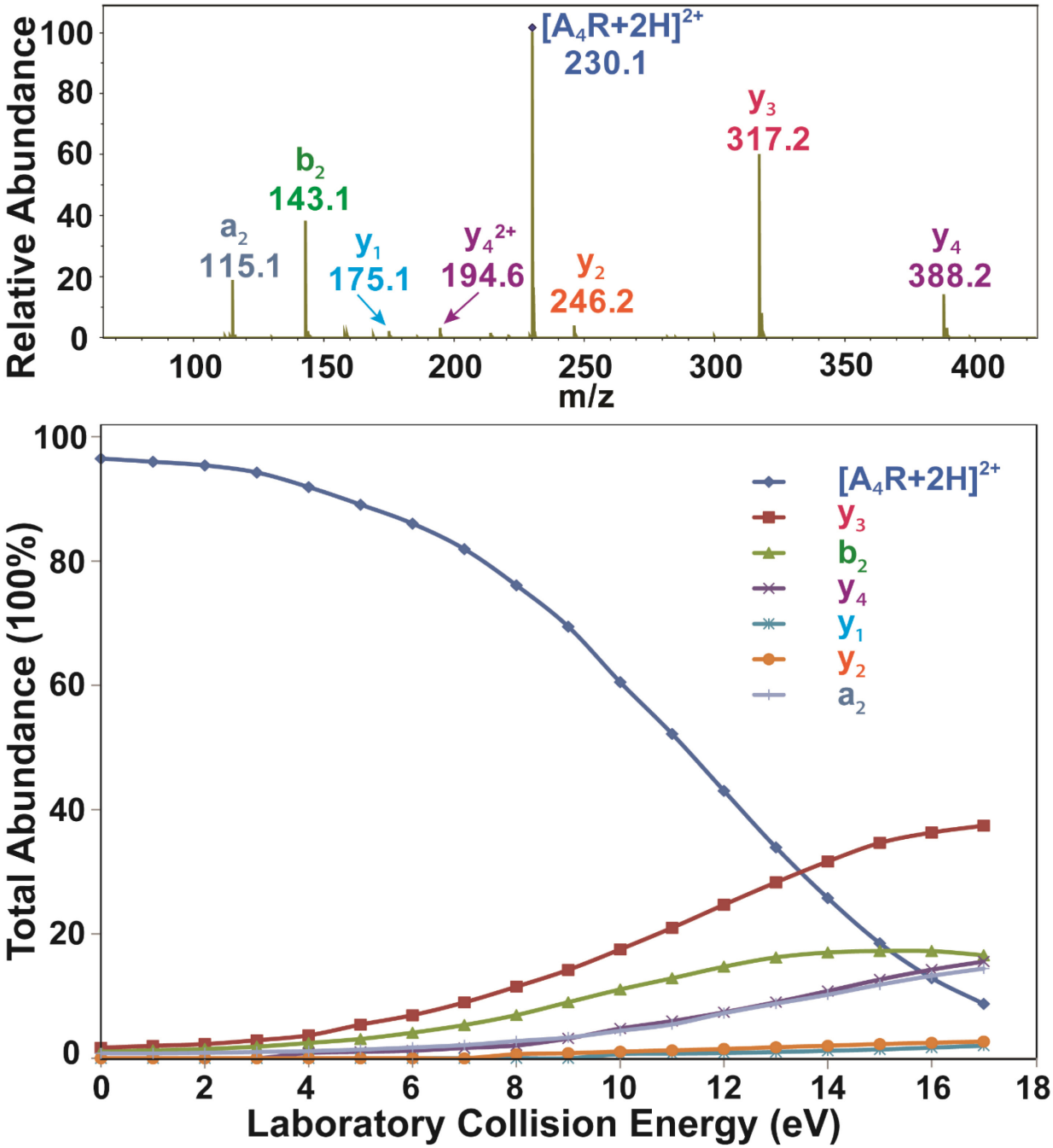

Figure 1. MS/MS of $[A_4R+2H]^{2+}$; the top panel is the MS/MS spectrum of $[A_4R+2H]^{2+}$ at laboratory collision energy of 12 eV, the bottom panel is the breakdown graph of $[A_4R+2H]^{2+}$.

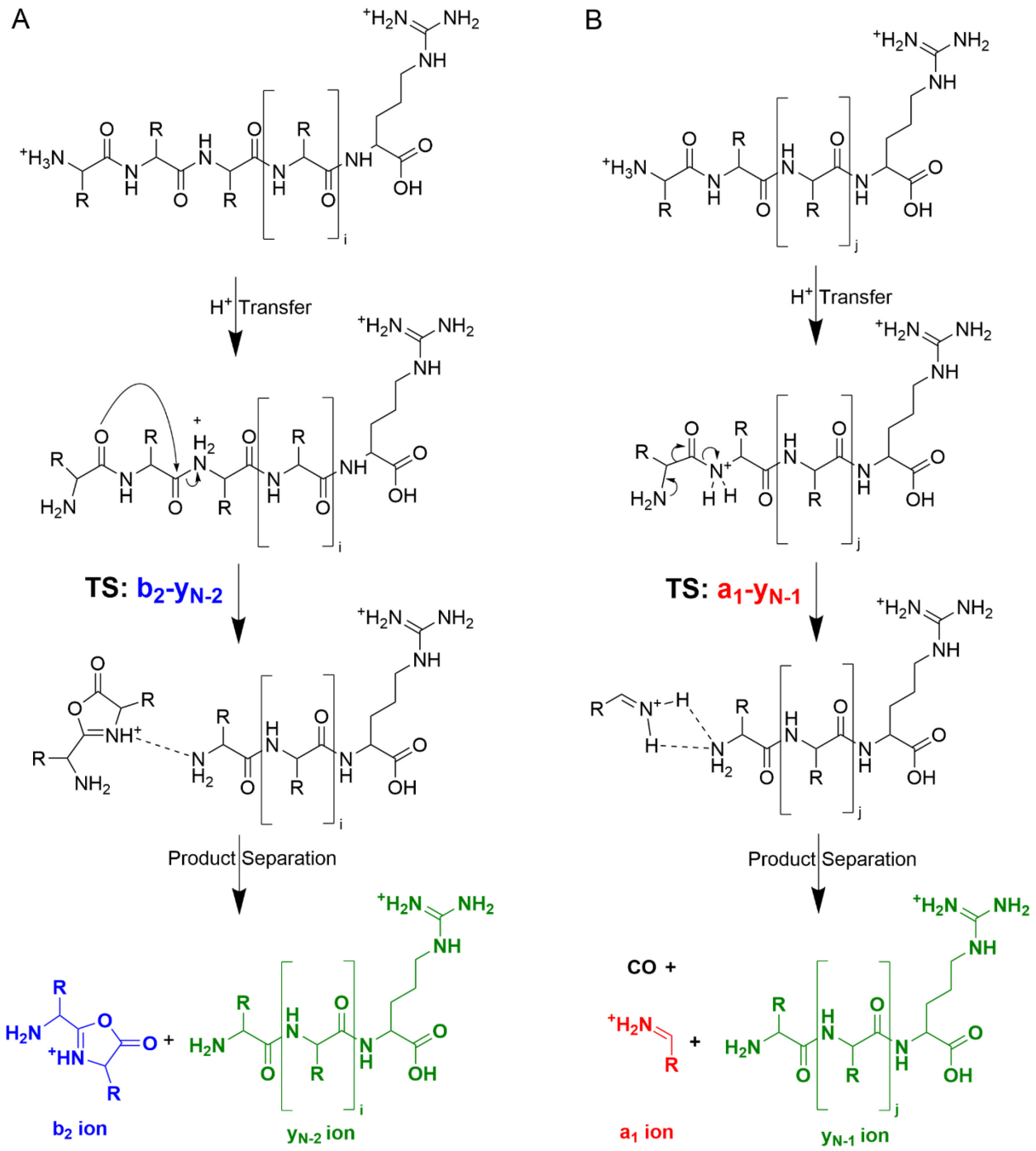

Scheme 1. Generic peptide fragmentation pathways for arginine terminated doubly protonated peptides: (A) b_2-y_{N-2} and (B) a_1-y_{N-1}. R is the amino acid side chain: H (glycine) or CH_3 (alanine) for the present analytes.

2. Comparison with Literature Analyses of Doubly Protonated Peptide Spectra

In the same manner as Shen et al. [48], the laboratory collision energies corresponding to 20, 50, and 80% of the peak current coming from fragments of the precursor ions were obtained from the breakdown graphs of each doubly protonated precursor peptide ion (denoted: E20, E50, and E80). Moderate linear correlations between these values and the degrees of freedom of the doubly protonated peptides were observed (R^2 = 0.44, 0.63, 0.73). None of these correlations explain anywhere near all the variance from linearity. Unsurprisingly, this suggests that factors other than ion size also influence peptide fragmentation. i.e., chemical structure and/or gas-phase dissociation chemistry matters.

While broadly instructive, the preceding analysis provides no specifics regarding which dissociations contributed to the agreement/variance. To get a more specific estimate of this we needed to parse the data into its individual channels. We separated the ion current for each of the peaks generated and compared the abundance of the fragment ions as a function of collision energy. We followed the approach of Stavitski et al. [37] by using the abundances of the y_m peaks as a surrogate for the order of preference of the corresponding amide bond cleavage. This choice minimizes the biases inherent in failing to detect low m/z peaks which are predominantly N-terminal fragments. [37] **Figure 2** illustrates the progression in product ion abundances as a function of analyte size and composition. The degree of charge-charge repulsion decreases down the columns as the analyte length increases (N = 3→6). Concomitantly, the size of the most abundant y_m peaks detected increases down the columns too. Across the $[G_xR+2H]^{2+}$ and $[A_xR+2H]^{2+}$ analyte series, the most dominant fragments are consistently the y_{N-1} and y_{N-2} peaks which correspond directly to the a_1-y_{N-1} and b_2-y_{N-2} fragmentation pathways. The preference between y_{N-1} and y_{N-2} ions appears to depend on the size of the precursor peptide ion; the 3 residue

systems produce higher abundance y_{N-1} ions whereas the 5 and 6 residue systems higher abundance y_{N-2} peaks at lower collision energies. The 4-residue systems are a mixture with the lighter $[G_3R+2H]^{2+}$ analytes consistently favoring the y_3 product over the y_2 product, whereas the heavier $[A_3R+2H]^{2+}$ analytes prefer the y_2 products at all but the highest collision energy. Consequently, the shortest peptides appear to be an exception to the general pattern identified by Stavitski et al. [37] in which shorter systems typically had the y_{N-2} peak as the most abundant (termed class I). We note that the earlier validated dataset [37] lacked peptides of length $N < 6$. The origins of this atypical behavior in shorter doubly protonated peptides will be discussed in the subsequent sections.

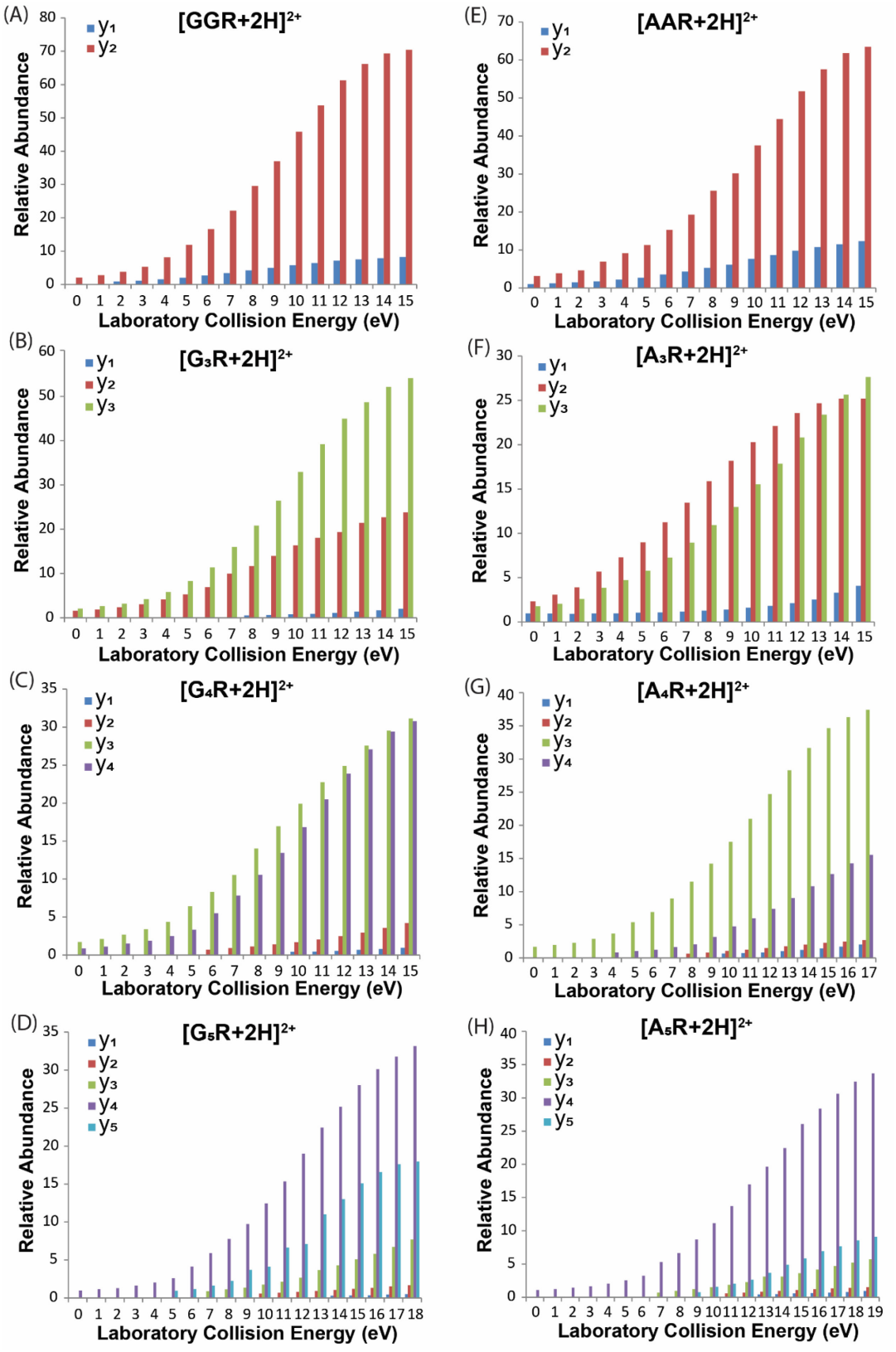

Figure 2. Relative abundances of y_m ions versus laboratory collision energy. The relative abundance of each y ion is the sum of singly and doubly charged forms.

Another interesting finding in Stavitski et al. was the substantial prevalence of the a_2 peak, particularly in comparison to the a_3 which was almost never detected. [37] Decarbonylation of b_n ions to form the corresponding a_n ions is well known [1–3, 10, 53, 63, 98, 103–105]. We see evidence of size-dependence of this fragmentation process in the relative abundances of b_2 and a_2 peaks formed from the $[A_xR+2H]^{2+}$ analytes (**Figure 3**) with the shorter sequences providing high proportions of a_2 peaks even at the lowest collision energies. In line with targeted experimental and theoretical work on Type I doubly protonated peptide ions [62], the longer sequences see a reduction in the relative b_2:a_2 ion current ratio at higher collision energies consistent with an increase in consecutive dissociation of the b_2 ions when more energy is available. The alternative possibility is that there is substantial activity in the a_2-y_{N-2} pathway for either these shorter doubly protonated peptide sequences at all collision energies, or from the longer sequences at higher collision energies. We address these competing processes and wider spectral interpretation in the following sections. Finally, we note that the comparatively low m/z of a_2 ions generated from the $[G_xR+2H]^{2+}$ sequences limit an unbiased, equivalent analysis as their abundances are likely underestimated by our instrument set up.

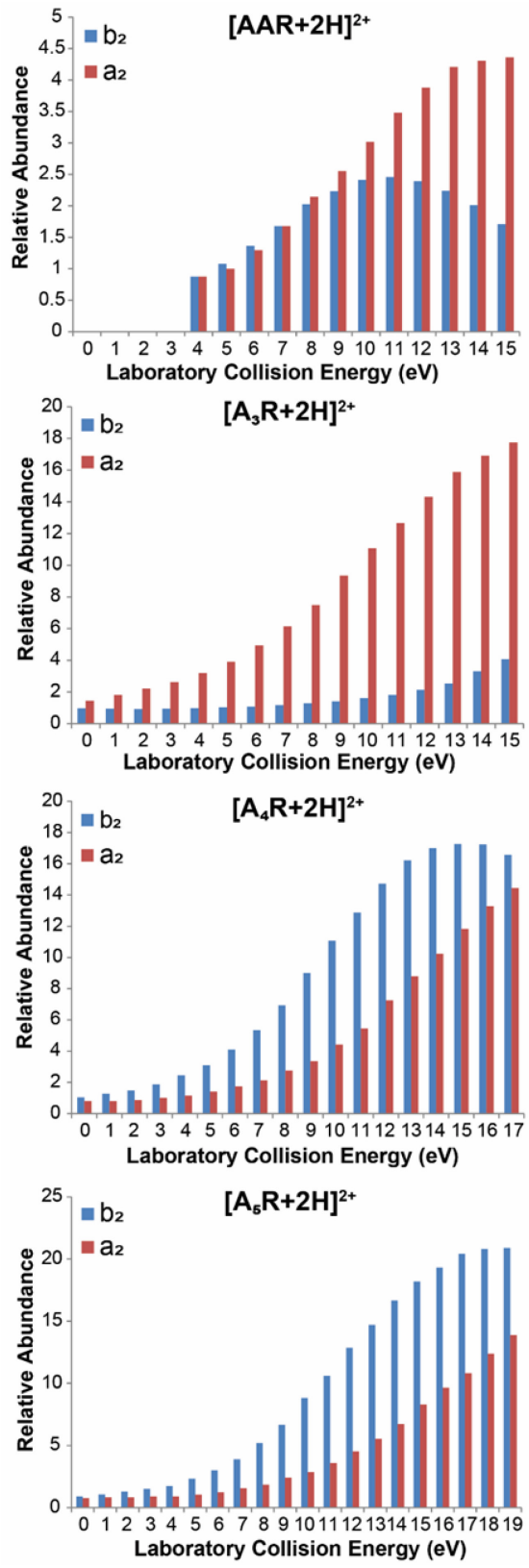

Figure 3. The relative abundances of b_2 and a_2 ions vs. the laboratory collision energy for doubly protonated A_xR (x=2-5) series.

3. *Density Functional Theory Threshold Energies to the Rescue?*

The primary dissociation channels of doubly protonated tryptic peptides are the a_n-y_m and b_n-y_m fragmentation pathways (Scheme 1). Both reaction types begin with mobilization of a proton to an amide nitrogen. This weakens the amide bond by removing the partial conjugation, facilitating amide bond cleavage reactions [64, 106]. Transfer of a proton to the first amide nitrogen enables the a_1-y_{N-1} fragmentation pathway to occur. y_{N-1} ions are generated by concerted cleavage of the amide and the CHR-CO bonds producing three fragments: a protonated imine ($RCH{=}NH_2^+$), CO, and the y_{N-1} ion, a protonated, truncated peptide. These fragments form a short-lived proton-bound dimer in which further proton transfers may occur prior to dissociation (and detection). The lifetime of this dimer and the likelihood of proton transfers between the fragments is determined by the energy available (degree of activation) and the composition of the constituent components. It is atypical to observe evidence of the b_1-y_{N-1} reaction as with a few notable exceptions [107–113], b_1 ions have acylium ion structures which are unstable with respect to decarbonylation [114]. In principle other a_n-y_m reactions can occur once protons are mobilized to other amide nitrogens producing product series. More commonly, we observe b_n ion series, evidence of b_n-y_m fragmentation pathways (Scheme 1).

The b_n-y_m fragmentation pathway also begins with proton mobilization. Population of any amide nitrogen site by an ionizing proton weakens the amide bond enabling nucleophilic attack into the electropositive carbonyl carbon by the preceding carbonyl oxygen with concerted amide bond cleavage. A protonated oxazolone derivative and a protonated, truncated peptide/amino acid ion are generated an initially held together in a proton bound dimer.[12, 72, 73, 115] Direct dissociation of the dimer produces singly charged b_n and y_m ions. Proton transfers prior to

dissociation can lead to doubly protonated species with a corresponding neutral (typically y_m^{2+} due to the presence of the basic residue R/K at the C-terminus of tryptic peptides).

Figure 2 illustrates the progression in doubly protonated peptide dissociation with the y_{N-1} than y_{N-2} peaks generally the most abundant fragmentation products. We used density function theory calculations at two levels of theory to model the competing reaction pathways and thereby identify theoretical energy thresholds for each doubly protonated peptide. Our calculations predict that the y_{N-1} ions are generated from the a_1-y_{N-1} fragmentation pathways and the y_{N-2} ions are produced by the lowest energy b_2-y_{N-2} pathways (Scheme 1). The lowest energy theoretical barriers of the potential a_1-y_{N-1} and b_2-y_{N-2} reactions are listed in **Tables S1 and S2**. Briefly, these values predict that the threshold relative energies ($\Delta E_{el+ZPE,\ 0K}$) for bond cleavages at the same site for peptides of different size are quite similar: (a) For the $[A_xR+2H]^{2+}$ analytes: the M06-2X model predicts the b_2-y_{N-2} reactions will require at least 157±5 (average±standard deviation) kJ mol^{-1} with the a_1-y_{N-1} reactions necessitating at least 192±6 kJ mol^{-1}. The $[G_xR+2H]^{2+}$ congeners require at least 157±6 (b_2-y_{N-2}) and 204±6 kJ mol^{-1} (a_1-y_{N-1}). (b) The B3LYP values make essentially the same prediction but differ in magnitude ($[A_xR+2H]^{2+}$: 135±15 and 167±8 kJ mol^{-1}; $[G_xR+2H]^{2+}$ 142±16 and 180±8 kJ mol^{-1}). In isolation, these findings are not consistent with experiment. Rather than dominance of the b_2-y_{N-2} pathway over the a_1-y_{N-1} pathway irrespective of analyte size, composition, or collision energy, we instead observe dominant y_{N-1} ion production in our shortest systems and increasing production of y_{N-1} ion current as a function of collision energy for the longer doubly protonated analytes. Thus, either the models are in error, or our instrument is operating in an energy regime substantially above the threshold energy (or both).

4. Size Dependent Entropic Changes and Unimolecular Dissociation Rate Constants

In all cases our B3LYP calculations predict the a_1-y_{N-1} reactions to be substantially more entropically favorable (by 51±13 J K^{-1} mol^{-1}) than the competing b_2-y_{N-2} pathways (Table S1). The effect has no clear relationship with analyte size. In contrast, the M06-2X entropic changes (Table S2) do vary with the peptide length. The relative entropies of the 3- and 4-residue analytes strongly favor the a_1-y_{N-1} reaction (by 65±13 J K^{-1} mol^{-1}) whereas the 5- and 6-residue systems moderately favor the b_2-y_{N-2} pathways (by 14±8 J K^{-1} mol^{-1}). These substantially larger ΔS values for the a_1-y_{N-1} reaction for the 3- and 4-residue peptides offer support for the hypothesis that all dissociations occur at energies substantially above the theoretical threshold. Thus, $\Delta G(T_{effective})$ would be the more pertinent value than ΔE_{0K}.[116–120] A more stringent test of this hypothesis is provided by calculation of RRKM unimolecular dissociation rate constants as a function of internal energy using the theoretical vibrational frequencies, rotational constants, and TS energies.

Example comparisons of the y_{N-1} and y_{N-2} ion current versus laboratory collision energy and RRKM unimolecular dissociation rate constant versus internal energy are provided in **Figure 4** (M06-2X data) for the $[A_xR+2H]^{2+}$ analyte series (Figure S3; $[G_xR+2H]^{2+}$). The RRKM data predict for the shortest, most charge dense system, $[A_2R+2H]^{2+}$, that despite the b_2-y_{N-2} pathway having a threshold energy 47 kJ mol^{-1} lower than the a_1-y_{N-1} TS (198 kJ mol^{-1}, Table S2) that the a_1-y_{N-1} reaction should predominate at both higher internal energy levels and shorter timescales (where $\log(k) \geq \sim 2.7$ or the analyte internal energy exceeds ~468 kJ mol^{-1}). Consequently, the relative abundances of the y_{N-1} and y_{N-2} peaks support these reactions occurring at energies well above threshold. The greatly differing slopes show that the rate constant for the a_1-y_2 reaction becomes larger than the b_2-y_1 reaction resulting in subsequent dominance of the a_1-y_2 pathway over the b_2-y_1 pathway consistent with experiment (Figure 4, first row). A similar prediction and

corresponding experimental progression can be seen for the $[A_3R+2H]^{2+}$ dissociations. The main difference is the a_1-y_{N-1} and b_2-y_{N-2} curves have more similar slopes (rate constants) which results in curve crossing at a higher degree of activation (log(k) ~4.3; internal energy ~530 kJ mol^{-1}). Consequently, the rates of reaction are similar initially with the y_{N-1} peak becoming increasingly competitive at higher collision energies (Figure 4, second row). For the longer doubly protonated peptides the RRKM data predicts that the y_{N-2} peak should be more abundant than y_{N-1} consistent with experiment. Additionally, these data indicate that more activation is necessary to substantially dissociate these systems as they increase in size in agreement with theory. [93, 117] These general findings were reproduced for the $[G_xR+2H]^{2+}$ systems with M06-2X (Figure S3). Thus, in terms of trends the M06-2X TSs combined with RRKM calculations provide a better qualitative match with experiment.

The RRKM calculations generated from the B3LYP structures were less consistent with experiment (Figures S4 and S5). For example, these calculations underpredict the rate constants for the b_2-y_{N-2} pathway of $[A_3R+2H]^{2+}$ which would result in both initial preference for and subsequent dominant production of y_3 ions rather than the similar abundances observed experimentally. In contrast, the shorter $[G_xR+2H]^{2+}$ analytes (3- and 4-residue) appear to underpredict the competitiveness of the a_1-y_{N-1} pathway while the longer analytes are predict substantially differing timescales for curve crossing despite relatively similar experimental results. In the next section we will discuss the physical origins of these apparent differences by examining the relevant transition structures and minima used in the RRKM calculations.

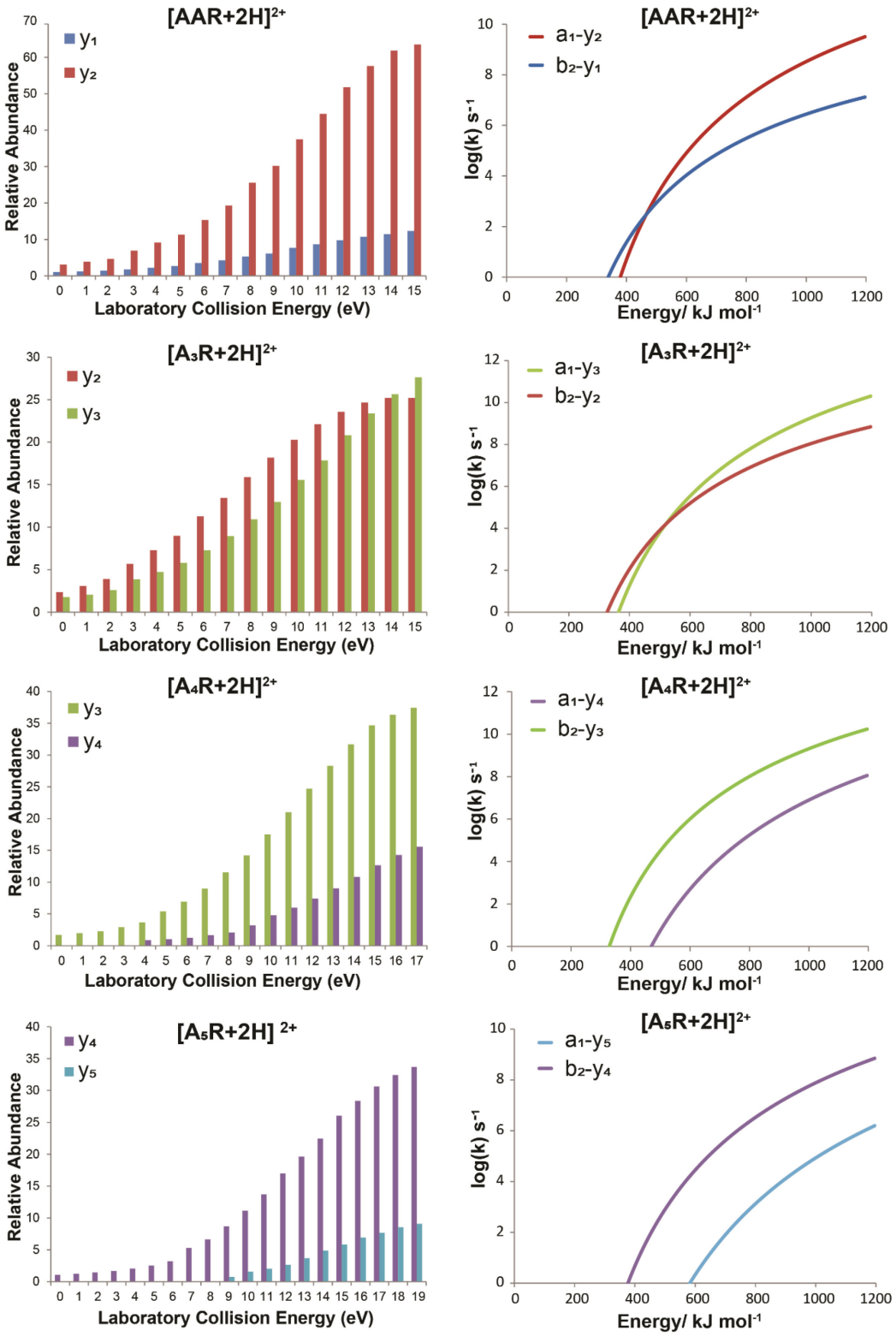

Figure 4. Left column: Relative abundances of y_{N-1} and y_{N-2} peaks as a function of collision energy for $[A_xR+2H]^{2+}$. Right column: RRKM plots for b_2-y_{N-2} and a_1-y_{N-1} reactions for $[A_xR+2H]^{2+}$ using data from M06-2X/6-31+G(d,p) calculations of global minima and TSs.

5. Structural Explanations, Charge-repulsion, and Different Chemical Models

Figures S6 and S7 show each of the conformations of the lowest energy minima of each of the $[A_xR+2H]^{2+}$ and $[G_xR+2H]^{2+}$ series. These are the reference structures for each set of relative energies and provide the vibrational states and rotational constants used in the denominator of the RRKM calculation. Consequently, these structures along with the transition structures determine the respective dissociation rates. The models differ markedly in their prediction of lowest energy structures. M06-2X minima are far more folded than their B3LYP congeners. Ergo, these structures have improved charge-solvation by making more hydrogen bonds at the cost of substantial decreases in the distances between the charge sites. i.e., increased coulombic repulsion. The other major difference is that B3LYP prefers protonation of the first carbonyl oxygen in all the tripeptide analytes, whereas M06-2X universally prefers to place the second ionizing proton at the N-terminus.

Based on the mobile proton model [4, 50, 121–123], one might expect both types of transition structures to necessitate mobilization of the N-terminal proton towards the C-terminus and thus reduction of the distance between the two charges with a concomitant increase in columbic repulsion and relative energy. Transition structures should thus favor more extended structures than the corresponding global minimum to limit charge-charge repulsion. The M06-2X transition structures (**Figures 5 and S6**) follow this prediction but are still substantially folded. More specifically, the M06-2X calculations indicate that for the small (3-, 4- residue) analyte ions, that the a_1-y_{N-1} transition structures are more extended and thus entropically better (ΔS is more positive) than the corresponding b_2-y_{N-2} transition structures (Figures 5 and S6). This is largely because of the size of these peptides means that fewer atoms are available to hydrogen bond and compensate for the charge-charge repulsion; adopting extended structures lowers the energy of the

transition structures. Concomitantly, formation of oxazolone rings in these shorter analytes limits the available conformations of the b_2-y_{N-2} transition structures making them entropically less favorable. The M06-2X transition structures for the longer analytes are far more folded and less entropically favorable resulting in the a_1-y_{N-1} and b_2-y_{N-2} reactions having much more similar ΔS values (Figures 5, S6, and Table S2). Consequently, the M06-2X data predict a substantial size dependence in the entropy changes of doubly protonated peptide fragmentation reactions. In contrast, the highly extended B3LYP minima structures have less room for additional extension to reduce charge-charge repulsion (Figures S5 and S6). The bond dissociation reactions calculated with B3LYP mainly predict structural changes around the bond cleavage sites rather than the whole peptide conformation. This is consistent with the B3LYP entropic values having less variance and size dependence than the M06-2X data.

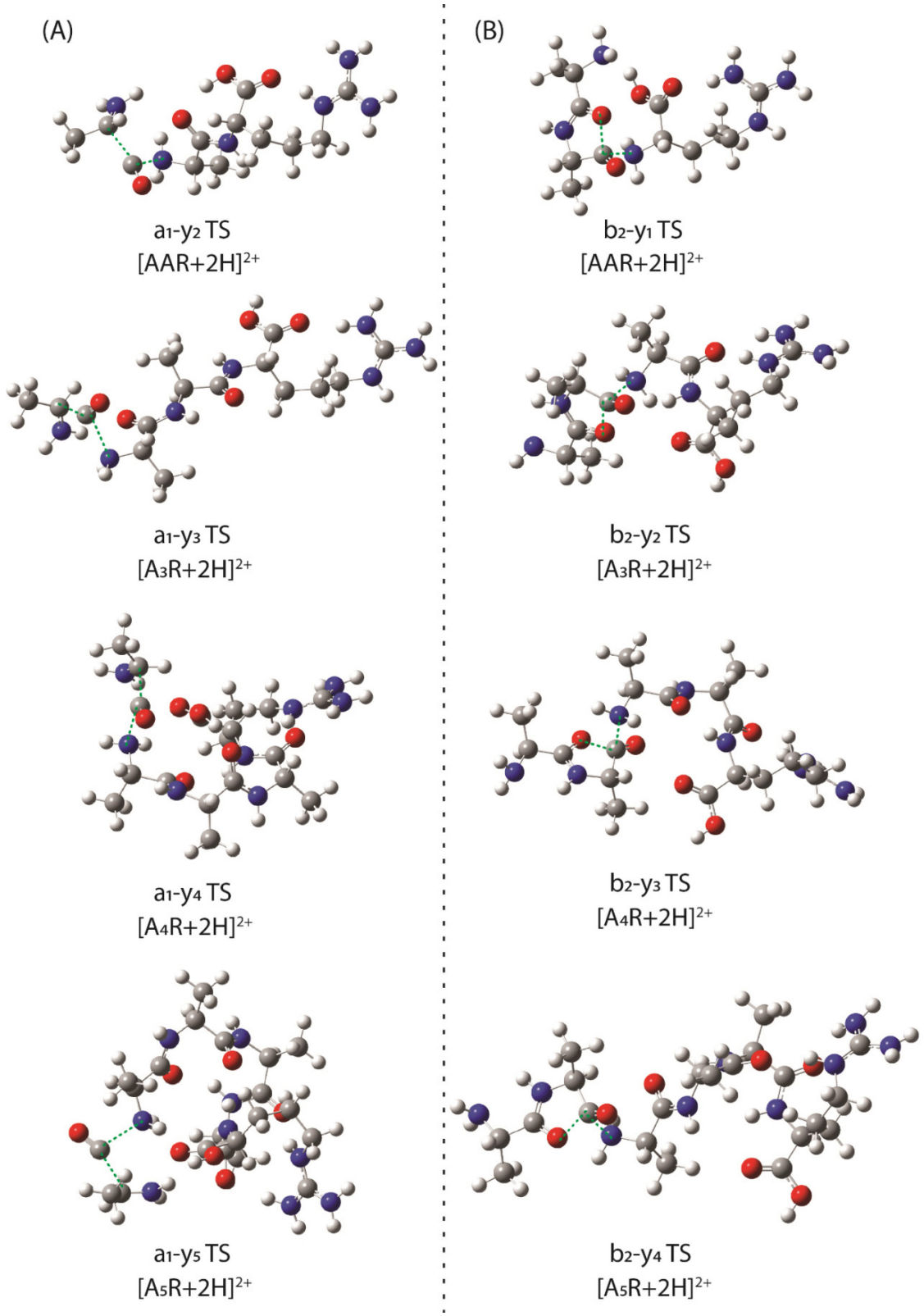

Figure 5. Transition structures of a_1-y_{N-1} and b_2-y_{N-2} reactions for $[A_xR+H]^+$ calculated at the M06-2X/6-31+G(d,p) level of theory.

6. Consecutive b_2-a_2 Dissociation Reactions Versus Analyte Length

Next, we briefly touch on potential consecutive dissociation of b_2 ions. Our experiments provide evidence of potential decarbonylation of b_2 ions to form the corresponding a_n ion (Scheme S1) to a substantial extent for the shorter $[A_xR+2H]^{2+}$ analytes (Figure 3) even at low collision energies. We tested this hypothesis with theory. Calculations at both the M06-2X and B3LYP levels of theory show this consecutive fragmentation pathway is spontaneous for $[A_xR+2H]^{2+}$ (x=2 or 3). i.e., the TS energies of the consecutive b_2-a_2 reactions were lower than the preceding b_2-y_{N-2} reaction (Tables S1-S4). Moreover, consecutive reactions are highly entropically favorable (ΔS = 180-280 J K^{-1} mol^{-1}, Tables S3 and S4) making these reactions even more likely. In contrast, for the larger $[A_xR+2H]^{2+}$ (x=4 or 5) ions, the secondary fragmentations require more energy than the preceding reactions. These theoretical predictions are consistent between levels of theory and with experiment.

7. Do additional Transition Structures Compete at Higher Effective Temperature?

Finally, based on a reviewer suggestion we completed further analyses of higher energy structures utilizing RRKM calculations. We investigated the possibility that higher energy, but entropically more favorable transition structures might also be competitive at increasing degree of activation (higher $T_{effective}$). Unsurprisingly, we found that these entropically more favorable TSs result in systematically steeper log(k) vs. Energy slopes for *both* the a_1-y_{N-1} and the b_2-y_{N-2} reactions. We found that the most competitive higher energy transition structures have barriers which are relatively similar to the lowest energy TSs (typically within ~20 kJ mol^{-1}) but also have more extended structures (ΔS => more positive). This combination results in increased rates at higher

internal energy compared to the lowest energy structures at 298 K. However, the relative rates of the 2 reactions are essentially unchanged resulting in minimal changes in overall description of each system. The exception to this is the smallest system ($[G_2R+2H]^{2+}$) where the RRKM plots for the M06-2X data substantially underpredict the competitiveness of the a_1-y_{N-1} pathway in comparison to experiment with the entropically favorable a_1-y_2 pathway only showing higher log(k) values beyond log(k) ≥ ~7.36 (analyte internal energy ~686 kJ mol^{-1}). This result is a more extreme form of the prior underprediction seen in Figure S3. As the smallest analyte this system should be most susceptible to changes to parameters used in the RRKM expression (vibrational frequencies, rotational constants).

Conclusions

We investigated the dissociation chemistry of 2 series of short, doubly charged tryptic peptides, ($[G_xR+2H]^{2+}$ and $[A_xR+2H]^{2+}$, x=2-5) experimentally and with theory. We find distinct differences in the preference of bond cleavage sites for these peptides as a function of size and to a lesser extent composition. Density functional calculations at two levels of theory predict that the threshold relative energies required for bond cleavages at the same site for peptides of different size are surprisingly similar. In isolation, this finding is inconsistent with experiment. However, the predicted extent of entropy change of these reactions is size dependent. RRKM rate calculations support this assertion and provide a general picture of the kinetics of the competing bond cleavage reactions enabling rationalization of experimental findings. The combined M06-2X data and RRKM modeling were consistent with experimental findings. These data showed substantial differences in the solvation and structure of the rate-determining transition structures

as a function of size. Shorter (3-, 4-residue) doubly protonated peptides access entropically favorable, extended a_1-y_{N-1} transition structures whereas longer (5-, 6-residue) peptides utilize more folded structures with more similar entropic characteristics to the competing b_2-y_{N-2} transition structures. The B3LYP data were far less consistent with experiment. However, the shorter doubly protonated peptides are also predicted to undergo spontaneous secondary dissociation of their b_2 ions to form of a_2 ions by both levels of theory consistent with experiment. Subsequent work will test the generality of these findings by extending the approach to encompass non-aliphatic residues (proline, aspartic acid, etc.).

ASSOCIATED CONTENT

Supporting Information

Supplementary Tables summarizing relative energetics, Figures, minima, and transition structure Figures are provided in the supporting PDF file. The Supporting Information is available free of charge on the ACS Publications website.

AUTHOR INFORMATION

Corresponding Author

*Benjamin Bythell, bythell@ohio.edu

Author Contributions

The manuscript was written through contributions of both authors.

ACKNOWLEDGMENT

This work was supported by start-up funds from Ohio University. SG was supported in-part by CHE-1948611. Calculations were performed at Ohio University and at the Missouri University of Science and Technology, Rolla, MO with support from the NSF (ACI-1919789). The authors thank Karl Irikura and 2 anonymous reviewers for helpful comments.

REFERENCES

1. Aebersold, R., Goodlett, D.R.: Mass spectrometry in proteomics. Chem Rev. 101, 269–296 (2001)
2. Aebersold, R., Mann, M.: Mass spectrometry-based proteomics. Nature. 422, 198–207 (2003)
3. Steen, H., Mann, M.: The abc's (and xyz's) of peptide sequencing. Nat Rev Mol Cell Biol. 5, 699–711 (2004)
4. Wysocki, V.H., Tsaprailis, G., Smith, L.L., Breci, L.A.: Mobile and localized protons: a framework for understanding peptide dissociation. J Mass Spectrom. 35, 1399–1406 (2000)
5. Tsaprailis, G., Nair, H., Somogyi, Á., Wysocki, V.H., Zhong, W., Futrell, J.H., Scott G. Summerfield, Gaskell, S.J.: Influence of secondary structure on the fragmentation of protonated peptides. J Am Chem Soc. 121, 5142–5154 (1999)
6. Summerfield, S.G., Gaskell, S.J.: Fragmentation efficiencies of peptide ions following low energy collisional activation. Int J Mass Spectrom Ion Process. 165–166, 509–521 (1997)
7. Burlet, O., Yang, C.Y., Gaskell, S.J.: Influence of cysteine to cysteic acid oxidation on the collision-activated decomposition of protonated peptides: evidence for intraionic interactions. J Am Soc Mass Spectrom. 3, 337–344 (1992)
8. Burlet, O., Orkiszewski, R.S., Ballard, K.D., Gaskell, S.J., Bertrand, M.J.: Charge promotion of low-energy fragmentations of peptide ions. Rapid Commun mass Spectrom. 6, 658–662 (1992)
9. Paizs, B., Suhai, S.: Fragmentation pathways of protonated peptides. Mass Spectrom Rev. 24, 508–548 (2005)
10. Papayannopoulos, I.A.: The interpretation of collision-induced dissociation tandem mass spectra of peptides. Mass Spectrom Rev. 14, 49–73 (1995)
11. Biemann, K.: Appendix 5. Nomenclature for peptide fragment ions (positive ions). Methods Enzymol. 193, 886–887 (1990)
12. Nold, M.J., Wesdemiotis, C., Yalcin, T., Harrison, A.G.: Amide bond dissociation in protonated peptides. Structures of the N-terminal ionic and neutral fragments. Int J Mass Spectrom Ion Process. 164, 137–153 (1997)
13. Barton, S.J., Whittaker, J.C.: Review of factors that influence the abundance of ions produced in a tandem mass spectrometer and statistical methods for discovering these factors. Mass Spectrom Rev. 28, 177–187 (2009)
14. Perkins, D.N., Pappin, D.J.C., Creasy, D.M., Cottrell, J.S.: Probability-based protein identification by searching sequence databases using mass spectrometry data. Electrophoresis. 20, 3551–3567 (1999)
15. Craig, R., Beavis, R.C.: TANDEM: matching proteins with tandem mass spectra. Bioinformatics. 20, 1466–1467 (2004)
16. Eng, J.K., McCormack, A.L., Yates, J.R.: An approach to correlate tandem mass spectral data of peptides with amino acid sequences in a protein database. J Am Soc Mass Spectrom. 5, 976–989 (1994)

17. Li, L., Sweedler, J. V.: Peptides in the brain: Mass spectrometry-based measurement approaches and challenges. Annu Rev Anal Chem. 1, 451–483 (2008)

18. Elias, J.E., Gibbons, F.D., King, O.D., Roth, F.P., Gygi, S.P.: Intensity-based protein identification by machine learning from a library of tandem mass spectra. Nat Biotechnol. 22, 214–219 (2004)

19. Lam, H., Deutsch, E.W., Aebersold, R.: Artificial decoy spectral libraries for false discovery rate estimation in spectral library searching in proteomics. J Proteome Res. 9, 605–610 (2010)

20. Cheng, C.Y., Tsai, C.F., Chen, Y.J., Sung, T.Y., Hsu, W.L.: Spectrum-based method to generate good decoy libraries for spectral library searching in peptide identifications. J Proteome Res. 12, 2305–2310 (2013)

21. Burke, M.C., Mirokhin, Y.A., Tchekhovskoi, D. V, Markey, S.P., Thompson, J.H., Larkin, C., Stein, S.E.: The hybrid search: a mass spectral library search method for discovery of modifications in proteomics. J Proteome Res. 16, 1924–1935 (2017)

22. Burke, M.C., Zhang, Z., Mirokhin, Y.A., Tchekovskoi, D. V., Liang, Y., Stein, S.E.: False discovery rate estimation for hybrid mass spectral library search identifications in bottom-up proteomics. J Proteome Res. 18, 3223–3234 (2019)

23. Zhou, C., Bowler, L.D., Feng, J.: A machine learning approach to explore the spectra intensity pattern of peptides using tandem mass spectrometry data. BMC Bioinformatics. 9, 325 (2008)

24. Kelchtermans, P., Bittremieux, W., Grave, K.D., Degroeve, S., Ramon, J., Laukens, K., Valkenborg, D., Barsnes, H., Martens, L.: Machine learning applications in proteomics research: How the past can boost the future. Proteomics. 14, 353–366 (2014)

25. Cao, X., Stojkovic, I., Obradovic, Z.: A robust data scaling algorithm to improve classification accuracies in biomedical data. BMC Bioinformatics. 17, 359 (2016)

26. Frank, A.M.: Predicting Intensity Ranks of Peptide Fragment Ions. J Proteome Res. 8, 2226–2240 (2009)

27. Frank, A., Pevzner, P.: PepNovo: de novo peptide sequencing via probabilistic network modeling. Anal Chem. 77, 964–973 (2005)

28. Zhang, Z.: Prediction of low-energy collision-induced dissociation spectra of peptides with three or more charges. Anal Chem. 77, 6364–6373 (2005)

29. Zhang, Z.: Prediction of low-energy collision-induced dissociation spectra of peptides. Anal Chem. 76, 3908–3922 (2004)

30. Li, W., O'Neill, H.A., Wysocki, V.H.: SQID-XLink: implementation of an intensity-incorporated algorithm for cross-linked peptide identification. Bioinformatics. 28, 2548–2550 (2012)

31. Li, W., Li, J., Goya, J., Tan, G., Wysocki, V.H.: SQID: An intensity-incorporated protein identification algorithm for tandem mass spectrometry. J Proteome Res. 10, 1593–1602 (2011)

32. Frank, A.M.: Predicting intensity ranks of peptide fragment ions. J Proteome Res. 8,

2226–2240 (2009)

33. Zhang, Z., Bordas-Nagy, J.: Peptide conformation in gas phase probed by collision-induced dissociation and its correlation to conformation in condensed phases. J Am Soc Mass Spectrom. 17, 786–794 (2006)

34. Haeffner, F., Merle, J.K., Irikura, K.K.: N-protonated isomers as gateways to peptide ion fragmentation. J Am Soc Mass Spectrom. 22, 2222–2231 (2011)

35. Huang, Y., Wysocki, V.H., Tabb, D.L., Yates, J.R.: The influence of histidine on cleavage C-terminal to acidic residues in doubly protonated tryptic peptides. Int J Mass Spectrom. 219, 233–244 (2002)

36. Barton, S.J., Richardson, S., Perkins, D.N., Bellahn, I., Bryant, T.N., Whittaker, J.C.: Using statistical models to identify factors that have a role in defining the abundance of ions produced by tandem MS. Anal Chem. 79, 5601–5607 (2007)

37. Savitski, M., Falth, M., Fung, Y., Adams, C., Zubarev, R.: Bifurcating fragmentation behavior of gas-Phase tryptic peptide dications in collisional activation. J Am Soc Mass Spectrom. 19, 1755–1763 (2008)

38. Huang, Y., Wysocki, V.H., Tabb, D.L., Yates, J.R.: The influence of histidine on cleavage C-terminal to acidic residues in doubly protonated tryptic peptides. Int J Mass Spectrom. 219, 233–244 (2002)

39. Breci, L.A., Tabb, D.L., Yates, J.R., Vicki H. Wysocki: Cleavage N-terminal to proline: analysis of a database of peptide tandem mass spectra. Anal Chem. 75, 1963–1971 (2003)

40. Schütz, F., Kapp, E.A., Simpson, R.J., Speed, T.P.: Deriving statistical models for predicting peptide tandem MS product ion intensities. Biochem Soc Trans. 31, 1479–83 (2003)

41. Kapp, E.A., Schütz, F., Reid, G.E., Eddes, J.S., Moritz, R.L., O'Hair, R.A.J., Speed, T.P., Simpson, R.J: Mining a tandem mass spectrometry database to determine the trends and global factors influencing peptide fragmentation. Anal Chem. 75, 6251–6264 (2003)

42. Tabb, D.L., Smith, L.L., Breci, L.A., Wysocki, V.H., Lin, D., Yates, J.R.: Statistical characterization of ion trap tandem mass spectra from doubly charged tryptic peptides. Anal Chem. 75, 1155–1163 (2003)

43. Huang, Y., Triscari, J.M., Pasa-Tolic, L., Anderson, G.A., Lipton, M.S., Smith, R.D., Wysocki: Dissociation behavior of doubly-charged tryptic peptides: correlation of gas-phase cleavage abundance with ramachandran plots. J Am Chem Soc. 126, 3034–3035 (2004)

44. Tabb, D.L., Huang, Y., Wysocki, V.H., John R. Yates: Influence of basic residue content on fragment ion peak intensities in low-energy collision-induced dissociation spectra of peptides. Anal Chem. 76, 1243–1248 (2004)

45. Huang, Y., Triscari, J.M., Tseng, G.C., Pasa-Tolic, L., Lipton, M.S., Smith, R.D., Wysocki, V.H.: Statistical characterization of the charge state and residue dependence of low-energy CID peptide dissociation patterns. Anal Chem. 77, 5800–5813 (2005)

46. Godugu, B., Neta, P., Simón-Manso, Y., Stein, S.E.: Effect of N-terminal glutamic acid

and glutamine on fragmentation of peptide ions. J Am Soc Mass Spectrom. 21, 1169–1176 (2010)

47. Harrison, A.G.: Charge-separation reactions of doubly-protonated peptides: Effect of peptide chain length. J Am Soc Mass Spectrom. 20, 1890–1895 (2009)

48. Shen, Y., Nemati, R., Wang, L., Yao, X.: Determining linear free energy relationships in peptide fragmentation using derivatization and targeted mass spectrometry. Anal Chem. 90, 1587–1594 (2018)

49. Paizs, B., Lendvay, G., Vékey, K., Suhai, S.: Formation of b2+ ions from protonated peptides: anab initio study. Rapid Commun Mass Spectrom. 13, 525–533 (1999)

50. Csonka, I.P., Paizs, B., Lendvay, G., Suhai, S.: Proton mobility in protonated peptides: a joint molecular orbital and RRKM study. Rapid Commun Mass Spectrom. 14, 417–431 (2000)

51. Paizs, B., Suhai, S.: Combined quantum chemical and RRKM modeling of the main fragmentation pathways of protonated GGG. I.cis-trans isomerization around protonated amide bonds. Rapid Commun Mass Spectrom. 15, 2307–2323 (2001)

52. Paizs, B., Suhai, S.: Combined quantum chemical and RRKM modeling of the main fragmentation pathways of protonated GGG. II. Formation of b2, y1, and y2 ions. Rapid Commun Mass Spectrom. 16, 375–389 (2002)

53. Aribi, H. E, Rodriquez, C.F., Almeida, D.R.P., Ling, Y., Mak, W.W.N., Hopkinson, A.C., Siu, K.W.M.: Elucidation of fragmentation mechanisms of protonated peptide ions and their products: a case study on glycylglycylglycine using density functional theory and threshold collision-induced dissociation. J Am Chem Soc. 123, 3006–3012 (2003)

54. O'Hair, R.A.J., Reid, G.E.: Neighboring group versus cis-elimination mechanisms for side chain loss from protonated methionine, methionine sulfoxide and their peptides. Eur Mass Spectrom. 5, 325–334 (1999)

55. Farrugia, J.M., Richard, A.J.: Involvement of salt bridges in a novel gas phase rearrangement of protonated arginine-containing dipeptides which precedes fragmentation. Int J Mass Spectrom. 222, 229–242 (2003)

56. O'Hair, R.A.J., Reid, G.E.: Does side chain water loss from protonated threonine yield N-protonated dehydroamino-2-butyric acid? Rapid Commun mass Spectrom. 12, 999–1002 (1998)

57. Paizs, B., Suhai, S.: Towards understanding the tandem mass spectra of protonated oligopeptides. 1: mechanism of amide bond cleavage. J Am Soc Mass Spectrom. 15, 103–113 (2004)

58. Obolensky, O.I., Wu, W.W., Shen, R.F., Yu, Y.K.: Using dissociation energies to predict observability of b- and y-peaks in mass spectra of short peptides. Rapid Commun Mass Spectrom. 26, 915–920 (2012)

59. Verkerk, U.H., Zhao, J., Van Stipdonk, M.J., Bythell, B.J., Oomens, J., Hopkinson, A.C., Siu, K.W.M.: Structure of the [M+ H–H2O]+ ion from tetraglycine: a revisit by means of density functional theory and isotope labeling. J Phys Chem A. 115, 6683–6687 (2011)

60. Obolensky, O.I., Wu, W.W., Shen, R., Yu, Y.: Using dissociation energies to predict observability of b-and y-peaks in mass spectra of short peptides. II. Results for hexapeptides with non-polar side chains. Rapid Commun Mass Spectrom. 27, 152–156 (2013)

61. Pechan, T., Gwaltney, S.R.: Calculations of relative intensities of fragment ions in the MSMS spectra of a doubly charged penta-peptide. BMC Bioinformatics. 13, S13 (2012)

62. Bythell, B.J., Somogyi, Á., Paizs, B., Somogyi, A.: What is the structure of b2 ions generated from doubly protonated tryptic peptides? J Am Soc Mass Spectrom. 20, 618–624 (2009)

63. Bythell, B.J., Erlekam, U., Paizs, B., Maître, P.: Infrared spectroscopy of fragments from doubly protonated tryptic peptides. ChemPhysChem. 10, 883–885 (2009)

64. Bythell, B.J., Suhai, S., Somogyi, A., Paizs, B.: Proton-driven amide bond-cleavage pathways of gas-phase peptide ions lacking mobile protons. J Am Chem Soc. 131, 14057–14065 (2009)

65. Bythell, B.J., Maître, P., Paizs, B.: Cyclization and rearrangement reactions of an fragment ions of protonated peptides. J Am Chem Soc. 132, 14766–14779 (2010)

66. Knapp-Mohammady, M., Young, A.B., Paizs, B., Harrison, A.G.: Fragmentation of doubly-protonated Pro-His-Xaa tripeptides: formation of b_2^{2+} ions. J Am Soc Mass Spectrom. 20, 2135–2143 (2009)

67. Bythell, B.J., Molesworth, S., Osburn, S., Cooper, T., Paizs, B., Van Stipdonk, M.: Structure and reactivity of a_n and a_n* peptide fragments investigated using isotope labeling, tandem mass spectrometry, and density functional theory calculations. J Am Soc Mass Spectrom. 19, 1788–1798 (2008)

68. Abutokaikah, M.T., Guan, S., Bythell, B.J.: Stereochemical sequence ion selectivity: proline versus pipecolic-acid-containing protonated peptides. J Am Soc Mass Spectrom. 28, 182–189 (2017)

69. Armentrout, P.B., Clark, A.A.: The simplest b_2^+ ion: determining its structure from its energetics by a direct comparison of the threshold collision-induced dissociation of protonated oxazolone and diketopiperazine. Int J Mass Spectrom. 316–318, 182–191 (2012)

70. Mookherjee, A., Van Stipdonk, M.J., Armentrout, P.B.: Thermodynamics and reaction mechanisms of decomposition of the simplest protonated tripeptide, triglycine: a guided ion beam and computational study. J Am Soc Mass Spectrom. 28, 739–757 (2017)

71. Sinha, R.K., Erlekam, U., Bythell, B.J., Paizs, B., Maître, P.: Diagnosing the protonation site of b 2 peptide fragment ions using IRMPD in the X–H (X = O, N, and C) stretching region. J Am Soc Mass Spectrom. 22, 1645–1650 (2011)

72. Yalcin, T., Khouw, C., Csizmadia, I.G., Peterson, M.R., Harrison, A.G.: Why are b ions stable species in peptide spectra? J Am Soc Mass Spectrom. 6, 1165–1174 (1995)

73. Yalcin, T., Csizmadia, I.G., Peterson, M.R., Harrison, A.G.: The structure and fragmentation of bn (n≥3) ions in peptide spectra. J Am Soc Mass Spectrom. 7, 233–242 (1996)

74. Oomens, J., Young, S., Molesworth, S., Stipdonk, M.: Spectroscopic evidence for an oxazolone structure of the b2 fragment ion from protonated tri-alanine. J Am Soc Mass Spectrom. 20, 334–339 (2009)

75. Yoon, S.H., Chamot-Rooke, J., Perkins, B.R., Hilderbrand, A.E., Poutsma, J.C., Wysocki, V.H.: IRMPD spectroscopy shows that AGG forms an oxazolone b 2 + ion. J Am Chem Soc. 130, 17644–17645 (2008)

76. Perkins, B.R., Chamot-Rooke, J., Yoon, S.H., Gucinski, A.C., Somogyi, A., Wysocki, V.H.: Evidence of diketopiperazine and oxazolone structures for HA b_2^+ ion. J Am Chem Soc. 131, 17528–17529 (2009)

77. Haeffner, F., Irikura, K.K.: N-protonated isomers and coulombic barriers to dissociation of doubly protonated Ala8Arg. J Am Soc Mass Spectrom. 28, 2170–2180 (2017)

78. Nelson, C.R., Abutokaikah, M.T., Harrison, A.G., Bythell, B.J.: Proton mobility in b_2 ion formation and fragmentation reactions of histidine-containing peptides. J Am Soc Mass Spectrom. 27, 487–497 (2016)

79. Tureček, F., Panja, S., Wyer, J.A., Ehlerding, A., Zettergren, H., Nielsen, S.B., Hvelplund, P., Bythell, B., Paizs, B.: Carboxyl-catalyzed prototropic rearrangements in histidine peptide radicals upon electron transfer: effects of peptide sequence and conformation. J Am Chem Soc. 131, 16472–16487 (2009)

80. Case, D.A., Pearlman, D.A., Caldwell, J.W., Cheatham III, T.E., Ross, W.S., Simmerling, C.L., Darden, T.A., Merz, K.M., Stanton, R. V, Cheng, A.L., Vincent, J.J., Crowley, M., Tsui, V., Radmer, R.J., Duan, Y., Pitera, J., Massova, I.G., Seibel, G.L., Singh, U.C., Weiner, P.K., Kollmann, P.A.: AMBER 99; University of California: San Francisco, 1999.

81. Marianski, M., Supady, A., Ingram, T., Schneider, M., Baldauf, C.: Assessing the accuracy of across-the-scale methods for predicting carbohydrate conformational energies for the examples of glucose and α-maltose. J Chem Theory Comput. 12, 6157–6168 (2016)

82. Supady, A., Blum, V., Baldauf, C.: First-principles molecular structure search with a genetic algorithm. J Chem Inf Model. 55, 2338–2348 (2015)

83. Halgren, T.A.: Merck molecular force field. I. Basis, form, scope, parameterization, and performance of MMFF94. J Comput Chem. 17, 490–519 (1996)

84. Halgren, T.A.: Merck molecular force field. II. MMFF94 van der Waals and electrostatic parameters for intermolecular interactions. J Comput Chem. 17, 520–552 (1996)

85. Halgren, T.A.: Merck molecular force field. III. Molecular geometries and vibrational frequencies for MMFF94. J Comput Chem. 17, 553–586 (1996)

86. Halgren, T.A., Nachbar, R.B.: Merck molecular force field. IV. conformational energies and geometries for MMFF94. J Comput Chem. 17, 587–615 (1996)

87. Halgren, T.A.: Merck molecular force field. V. Extension of MMFF94 using experimental data, additional computational data, and empirical rules. J Comput Chem. 17, 616–641 (1996)

88. Frisch, M.J., Trucks, G.W., Schlegel, H.B., Scuseria, G.E., Robb, M.A., Cheeseman, J.R., Scalmani, G., Barone, V., Mennucci, B., Petersson, G.A.: Gaussian 09; Gaussian, Inc. Wallingford, CT. 32, 5648–5652 (2009)

89. Becke, A.D.: Density-functional thermochemistry. III. The role of exact exchange. J Chem Phys. 98, 5648–5652 (1993)

90. Lee, C., Yang, W., Parr, R.G.: Development of the Colle-Salvetti correlation-energy formula into a functional of the electron density. Phys Rev B. 37, 785–789 (1988)

91. Zhao, Y., Truhlar, D.G.: The M06 suite of density functionals for main group thermochemistry, thermochemical kinetics, noncovalent interactions, excited states, and transition elements: two new functionals and systematic testing of four M06-class functionals and 12 other function. Theor Chem Acc. 120, 215–241 (2008)

92. Zhao, Y., Schultz, N.E., Truhlar, D.G.: Exchange-correlation functional with broad accuracy for metallic and nonmetallic compounds, kinetics, and noncovalent interactions. J Chem Phys. 123, 161103 (2005)

93. Gilbert, R.G., Smith, S.C.: Theory of unimolecular and recombination reactions. (1990)

94. Lifshitz, C.: Some recent aspects of unimolecular gas phase ion chemistry. Chem Soc Rev. 30, 186–192 (2001)

95. Beyer, T., Swinehart, D.F.: Algorithm 448: number of multiply-restricted partitions. Commun ACM. 16, 379 (1973)

96. Becke, A.D.: Correlation energy of an inhomogeneous electron gas: a coordinate-space model. J Chem Phys. 88, 1053–1062 (1988)

97. Grimme, S.: Semiempirical GGA-type density functional constructed with a long-range dispersion correction. J Comput Chem. 27, 1787–1799 (2006)

98. Bythell, B.J., Harrison, A.G.: Formation of a1 ions directly from oxazolone b2 ions: an energy-resolved and computational study. J Am Soc Mass Spectrom. 26, 774–781 (2015)

99. Bleiholder, C., Paizs, B.: Competing gas-phase fragmentation pathways of asparagine-, glutamine-, and lysine-containing protonated dipeptides. Theor Chem Acc. 125, 387–396 (2010)

100. Bythell, B.J., Barofsky, D.F., Pingitore, F., Polce, M.J., Wang, P., Wesdemiotis, C., Paizs, B.: Backbone cleavages and sequential loss of carbon monoxide and ammonia from protonated AGG: a combined tandem mass spectrometry, isotope labeling, and theoretical study. J Am Soc Mass Spectrom. 18, 1291–1303 (2007)

101. Laerdahl, J.K., Uggerud, E.: Gas phase nucleophilic substitution. Int J Mass Spectrom. 214, 277–314 (2002)

102. Gritsenko, O. V, Ensing, B., Schipper, P.R.T., Baerends, E.J.: Comparison of the accurate Kohn−Sham solution with the generalized gradient approximations (GGAs) for the SN2 Reaction F-+ CH3F→ FCH3+ F-: a qualitative rule to predict success or failure of GGAs. J Phys Chem A. 104, 8558–8565 (2000)

103. Paizs, B., Szlávik, Z., Lendvay, G., Vékey, K., Suhai, S.: Formation of a2+ ions of protonated peptides. An ab initio study. Rapid Commun Mass Spectrom. 14, 746–755

(2000)

104. Mookherjee, A., Armentrout, P.B.: Thermodynamics and reaction mechanisms for decomposition of a simple protonated tripeptide, H+GAG: a guided ion beam and computational study. J Am Soc Mass Spectrom. 30, 1013–1027 (2019)

105. Oomens, J., Young, S., Molesworth, S., van Stipdonk, M.: Spectroscopic evidence for an oxazolone structure of the b2 fragment ion from protonated tri-alanine. J Am Soc Mass Spectrom. 20, 334–339 (2009)

106. Somogyi, Á., Wysocki, V.H., Mayer, I.: The effect of protonation site on bond strengths in simple peptides: application of ab initio and modified neglect of differential overlap bond orders and modified neglect of differential overlap energy partitioning. J Am Soc Mass Spectrom. 5, 704–717 (1994)

107. Yalcin, T., Harrison, A.G.: Ion chemistry of protonated lysine derivatives. J mass Spectrom. 31, 1237–1243 (1996)

108. Tsang, C.W., Harrison, A.G.: Chemical ionization of amino acids. J Am Chem Soc. 98, 1301–1308 (1976)

109. Tu, Y., Harrison, A.G.: The b1 ion derived from methionine is a stable species. Rapid Commun mass Spectrom. 12, 849–851 (1998)

110. Kulik, W., Heerma, W.: A study of the positive and negative ion fast atom bombardment mass spectra of α-amino acids. Biomed Environ Mass Spectrom. 15, 419–427 (1988)

111. Zou, S., Oomens, J., Polfer, N.C.: Competition between diketopiperazine and oxazolone formation in water loss products from protonated ArgGly and GlyArg. Int J Mass Spectrom. 316, 12–17 (2012)

112. Farrugia, J.M., Richard, A.J., Reid, G.E.: Do all b2 ions have oxazolone structures? Multistage mass spectrometry and ab initio studies on protonated N-acyl amino acid methyl ester model systems. Int J Mass Spectrom. 210, 71–87 (2001)

113. Bythell, B.J., Csonka, I.P., Suhai, S., Barofsky, D.F., Paizs, B.: Gas-phase structure and fragmentation pathways of singly protonated peptides with N-terminal arginine. J Phys Chem B. 114, 15092–15105 (2010)

114. Harrison, A.G.: To b or not to b: The ongoing saga of peptide b ions. Mass Spectrom Rev. 28, 640–654 (2009)

115. Cordero, M.M., Houser, J.J., Wesdemiotis, C.: Neutral products formed during backbone fragmentations of protonated peptides in tandem mass spectrometry. Anal Chem. 65, 1594–1601 (1993)

116. Rabus, J.M., Abutokaikah, M.T., Ross, R.T., Bythell, B.J.: Sodium-cationized carbohydrate gas-phase fragmentation chemistry: influence of glycosidic linkage position. Phys Chem Chem Phys. 19, 25643–25652 (2017)

117. Vékey, K.: Internal energy effects in mass spectrometry. J Mass Spectrom. 31, 445–463 (1996)

118. Carl, D.R., Chatterjee, B.K., Armentrout, P.B.: Threshold collision-induced dissociation of Sr 2+(H 2 O) x complexes (x= 1–6): an experimental and theoretical investigation of

the complete inner shell hydration energies of Sr 2+. J Chem Phys. 132, 44303 (2010)

119. Molina, E.R., Eizaguirre, A., Haldys, V., Urban, D., Doisneau, G., Bourdreux, Y., Beau, J., Salpin, J., Spezia, R.: Characterization of protonated model disaccharides from tandem mass spectrometry and chemical dynamics simulations. ChemPhysChem. 18, 2812–2823 (2017)

120. Heaton, A.L., Armentrout, P.B.: Thermodynamics and mechanism of the deamidation of sodium-bound asparagine. J Am Chem Soc. 130, 10227–10232 (2008)

121. Paizs, B., Csonka, I.P., Lendvay, G., Suhai, S.: Proton mobility in protonated glycylglycine and N-formylglycylglycinamide: a combined quantum chemical and RKKM study. Rapid Commun Mass Spectrom. 15, 637–650 (2001)

122. Harrison, A.G., Yalcin, T.: Proton mobility in protonated amino acids and peptides. Int J Mass Spectrom Ion Process. 165–166, 339–347 (1997)

123. Dongré, A.R., Jones, J.L., Somogyi, Á., Wysocki, V.H.: Influence of peptide composition, gas-phase basicity, and chemical modification on fragmentation efficiency: evidence for the mobile proton model. J Am Chem Soc. 118, 8365–8374 (1996)